

# Growth of ZnO nanotube arrays and nanotube based piezoelectric nanogenerators

Yi Xi,<sup>ab</sup> Jinhui Song,<sup>a</sup> Sheng Xu,<sup>a</sup> Rusen Yang,<sup>a</sup> Zhiyuan Gao,<sup>a</sup> Chenguo Hu<sup>\*b</sup> and Zhong Lin Wang<sup>\*a</sup>

Received 25th August 2009, Accepted 2nd October 2009

First published as an Advance Article on the web 29th October 2009

DOI: 10.1039/b917525c

We present a systematic study of the growth of hexagonal ZnO nanotube arrays using a solution chemical method by varying the growth temperature (<100 °C), time and solution concentration. A piezoelectric nanogenerator using the as-grown ZnO nanotube arrays has been demonstrated for the first time. The nanogenerator gives an output voltage up to 35 mV. The detailed profile of the observed electric output is understood based on the calculated piezoelectric potential in the nanotube with consideration of the Schottky contact formed between the metal tip and the nanotube; and the mechanism agrees with that proposed for nanowire based nanogenerator. Our study shows that ZnO nanotubes can also be used for harvesting mechanical energy.

## Introduction

Energy shortage and global warming are two grand challenges to human beings in the near future.<sup>1–3</sup> Solar cells, fuel cells, thermoelectric and piezoelectric technologies have drawn increasing attention due to their potential for converting photon, chemical, thermal and mechanical energies into electrical energy. Zinc oxide (ZnO) is a typical II–VI semiconductive and piezoelectric material with applications in electronics, optoelectronics, sensors, and energy conversions.<sup>4–6</sup> One-dimensional nanostructures of ZnO are very important semiconductor building blocks with unique and novel physical and chemical properties. Various morphologies of ZnO nanostructures, such as nanowire arrays,<sup>7</sup> nanorods,<sup>8</sup> nanobelts<sup>9,10</sup> and nanotubes,<sup>11</sup> have been synthesized using physical, chemical and electrochemical methods.

As for energy harvesting, ZnO nanowire (NW) array based piezoelectric nanogenerators have been demonstrated to convert mechanical energy into electricity by utilizing the coupled semiconducting and piezoelectric properties of ZnO.<sup>2,3,12,13</sup> Although the nanotubular structure of ZnO has become a popular topic, ZnO nanotube arrays have not yet been exploited for piezoelectric nanogenerator applications. In this communication, hexagonal ZnO nanotube arrays were synthesized at temperature less than 100 °C by solution chemical method, and were systematically studied under different growth conditions. The piezoelectric nanogenerators using ZnO nanotube arrays were demonstrated for the first time. Details of the output electrical signals from the nanogenerator were studied in reference to the calculated profile of piezoelectric potential for the nanotube geometry. Our results showed that the nanotubes have equivalent performance as the nanowires for energy conversion at least in the magnitude of the output voltage.

## Experimental method

In our experiments, (0001) GaN thin film grown on sapphire surfaces was chosen as the substrate for growing ZnO nanotubes. The close lattice match and structure match between GaN and ZnO allow a good control over the orientation of the ZnO nanotubes. GaN substrate was cleaned by a standard cleaning process. First, GaN substrate was ultrasonicated consecutively in acetone, ethanol, IPA (isopropyl alcohol), and de-ionized water for 5 min, respectively; then it was blown dry with nitrogen gas to eliminate any adsorbed moisture. The next step was to prepare the nutrient solution. The nutrient solution was composed of a 1 : 1 ratio of zinc nitrate to hexamethylenetetramine (HMTA). Both of the chemicals were reagent grade from Fluka (St. Louis, MO). The substrate was put face down at the top of the nutrient solution surface.<sup>14</sup> The reaction vessel was heated to 95 °C and kept at 95 °C for 2–3 h and then heated to 50 °C and kept at 50 °C for 3–48 h, and finally was allowed to cool down naturally. The current synthesis route has manifested the unique advantage of being without any post-treatment or any surfactant. The products were examined using a LEO 1530 scanning electron microscope (SEM).

## Results and discussion

The evolution of the morphology of the ZnO nanotube arrays on the GaN substrate has been studied under different growth conditions. The length of the ZnO nanotube arrays was tuned by controlling the reaction conditions such as temperature, concentration, and reaction time. Fig. 1a–d display SEM images of ZnO nanotube arrays that were first grown at 95 °C for 3 h and followed with growth at 50 °C for different lengths of time (3, 13, 16 and 21 h, respectively) during which the nutrient solution concentration was kept at 20 mmol L<sup>-1</sup>. The insets in Fig. 1 are the corresponding high-magnification SEM images, showing the shape of the ZnO nanotubes received under different conditions. The length of nanotubular structure was increased when the growth time was extended, but there was no significant change in their diameters (500–800 nm) and wall thickness (50–100 nm).

<sup>a</sup>School of Materials Science and Engineering, Georgia Institute of Technology, Atlanta, Georgia 30332-0245, USA. E-mail: zhwang@gatech.edu; hucg@cqu.edu.cn

<sup>b</sup>Department of Applied Physics, Chongqing University, Chongqing 400044, P.R. China

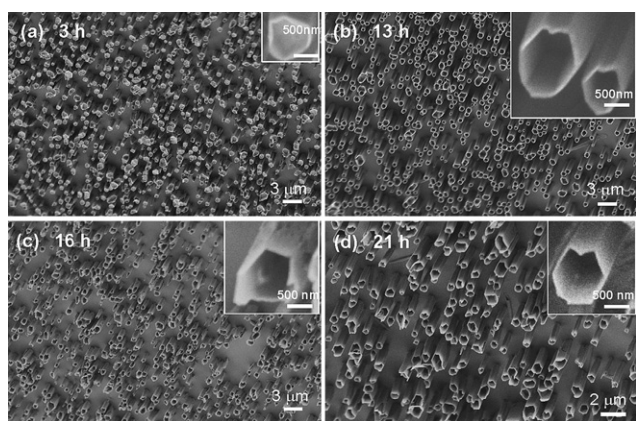


**Fig. 1** A series of SEM images of ZnO nanotube arrays grown with a concentration of 20 mmol L<sup>-1</sup>, and first at 95 °C for 3 h then at 50 °C for (a) 3 h, (b) 13 h, (c) 16 h and (d) 21 h, showing the graduated etching from nanorods into nanotubes. The insets are their corresponding higher-resolution SEM images, respectively.

The SEM images of the nanotubes grown under different concentrations (5, 15, 20, 25 and 30 mmol L<sup>-1</sup>) but at the same temperature and growth time (95 °C (3 h) then 50 °C (16 h)) are presented in Fig. 2. Fig. 2a indicates that the ZnO nanotube arrays hardly grew when the concentration was 5 mmol L<sup>-1</sup>. The first sight of ZnO nanotube formation was when the concentration reached 15 mmol L<sup>-1</sup> in Fig. 2b. But when the concentration was higher than 30 mmol L<sup>-1</sup> in Fig. 2e, the tube shape was largely distorted. This result indicates that the nutrient concentration in the reaction solution was found to be too low to induce any ZnO nanotube growth. This means when the nutrient concentration is 20 and 25 mmol L<sup>-1</sup>, a better morphology control over the ZnO nanotube arrays can be attained.

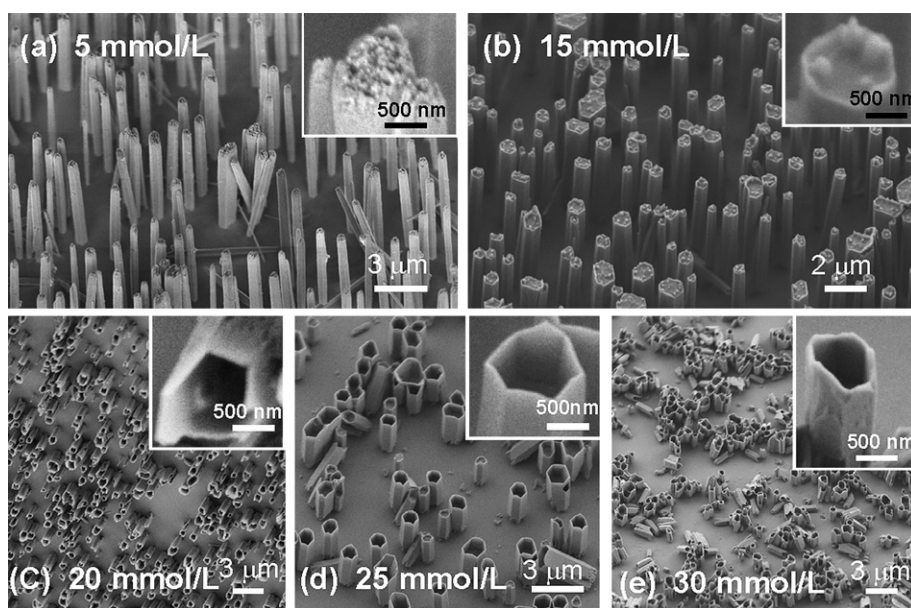


**Fig. 2** A series of SEM images of ZnO nanotube arrays grown first at 95 °C for 3 h and then at 50 °C for 16 h with a solution concentration of (a) 5, (b) 15, (c) 20, (d) 25, and (e) 30 mmol L<sup>-1</sup>. The insets are their corresponding higher-resolution SEM images, respectively.

The growth temperature can largely affect the growth morphology. A set of experiments that were carried out for a fixed growth time (2 h) but at two set temperatures during the entire growth process is shown in Fig. 3. Fig. 3a shows the growth that was first carried out at 95 °C (2 h) then at 50 °C (4 h). Fig. 3b–d show the growth that was carried out at 95 °C (2 h) then 65 °C (19 h), 105 °C (2 h) then 65 °C (41 h), and 105 °C (2 h) then 50 °C (3 h), respectively. It is apparent that the growth morphology is largely determined by the growth temperatures. The result indicates that the best growth conditions for forming ZnO nanotube arrays were when the temperature was kept at 95 °C then at 50 °C.

The as-grown nanotubes are single crystals and each of which has a growth direction of wurtzite [0001]. Fig. 4 shows the representative X-ray diffraction (XRD) spectrum recorded with

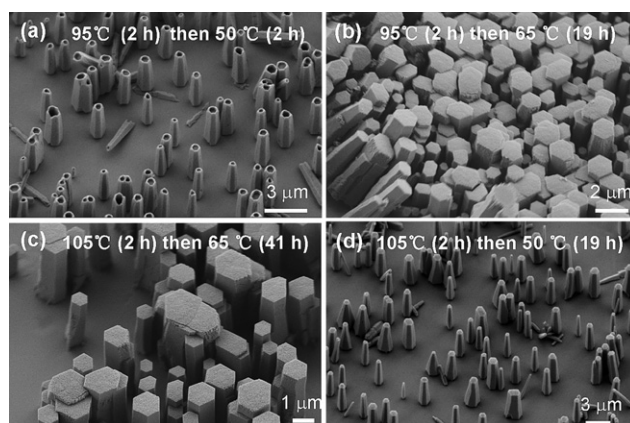


**Fig. 3** A series of SEM images of ZnO nanotube arrays grown at a solution concentration of 20 mmol L<sup>-1</sup> at different temperature and time settings as indicated.

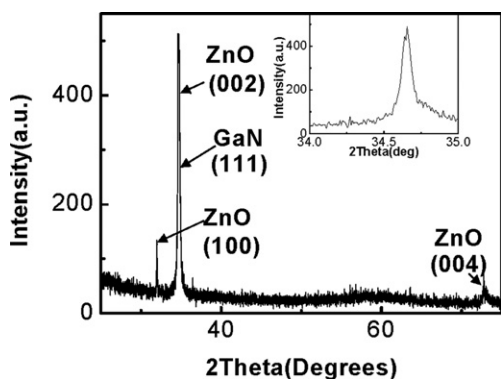
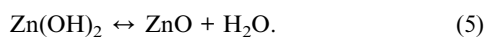
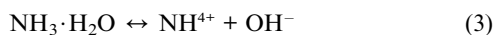
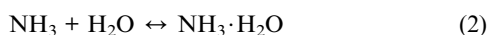


**Fig. 4** An X-ray diffraction pattern of the as-grown ZnO nanotube arrays on GaN (111) with the incident X-ray beam normal to the substrate. Inset is the ZnO (0002) peak rocking curve.

the incident X-ray normal to the substrate. As shown in the pattern, all of the diffraction peaks match the ZnO structure, with lattice structure of  $a = 3.248 \text{ \AA}$  and  $c = 5.205 \text{ \AA}$ . The dominant appearance of the (0002) and (0004) peaks of ZnO shows its orientation relationship. The hexagonal shapes of the nanotubes as revealed by the SEM images are consistent with the XRD data. A weak (10–10) peak of ZnO as observed in XRD spectrum shows that there were some flipped over tubes on the substrates, which were captured by SEM.

The nanotubes were grown possibly following the reactions listed below:<sup>14</sup>



The growth process of the ZnO nanotube arrays could be divided into two stages.<sup>15,16</sup> The first growth stage corresponds to the precipitation of ZnO nanorod arrays at a higher temperature (95 °C). It is well-known that the hexagonal ZnO crystal has both polar and non-polar faces. The oxygen-terminated (000 $\bar{1}$ ) and the zinc-terminated (0001) are the typical polar surfaces. The non-polar faces are composed of the low-index faces (parallel to the  $c$  axis), such as  $\{1\bar{0}10\}$  and  $\{1\bar{1}20\}$ . Non-polar faces are more stable than the metastable polar faces.<sup>16</sup> At the early stage of the reaction, the growth units ( $\text{ZnO}_2^{2-}$ ) in the solution near the surface of ZnO nuclei are likely adsorbed on the positive polar faces of the (0001) surface; and a faster growth along the [0001] direction forms nanorods.<sup>17</sup> The second stage is an etching process, which is called the aging process and corresponds to the dissolution of ZnO nanorod arrays at a lower temperature (50 °C). In this case, the preferential chemical dissolution of the metastable (0001) faces of the fully grown oriented nanorods shall lead to the required highly porous and oriented non-polar hollow structure.<sup>18</sup> (0001) surface can terminate with either  $\text{Zn}^{2+}$  or  $\text{O}^{2-}$ , which is a polar surface with surface charges and tends to

be more reactive. At a low temperature such as 50 °C, the dissolution rate may be larger than the precipitation rate. Thus, the polar surface is likely to be etched by the residual chemicals, forming the tubular geometry. The aging conditions are such that the systems will tend to reach their thermodynamic stability and may undergo variation in morphology and size.<sup>16</sup>

The piezoelectric energy conversion of the nanotubes was first characterized by atomic force microscopy (AFM) (Molecular Force Probe MFP-ED from Asylum Research) with a Pt coated Si tip in contact mode. Details of the nanogenerator's demonstration and the measurement of this can be found in ref. 2 and 12. In the AFM contact mode, a constant normal force of  $\sim 80 \text{ nN}$  was maintained between the tip and nanotubes. The rectangular AFM cantilever had a calibrated normal spring constant of  $1.857 \text{ N m}^{-1}$ . A voltage drop across an external load of  $500 \text{ M}\Omega$  connected to the AFM cantilever and tip was continuously monitored when the tip scanned across the sample. The electric voltage measured over the load is produced by the transient electric current created by the piezoelectric potential in the nanotube as a result of AFM tip induced mechanical deformation. In our experiment, the AFM tip has an apex angle of  $70^\circ$ . Fig. 5a demonstrates a 3D plot of topographic image received when scanning the AFM tip in contact mode over an area of  $20 \mu\text{m} \times 20 \mu\text{m}$  of the vertically aligned ZnO nanotubes. The scanning direction was from right to left. The shapes of some nanotubes can be resolved in the AFM image. Corresponding to this AFM topography image, a 3D plot of the voltage output image captured over the external load is exhibited in Fig. 5b, from which it can be seen that there were a number of sharp peaks with amplitudes ranging from 10 to 35 mV. The magnitude of this voltage output is in the same range as that received for ZnO nanowires,<sup>1,2,12,13</sup> and of course it depends on the size of the nanostructure. The negative voltage peaks in reference to the grounded sample substrate are consistent with those received for ZnO nanowires,<sup>2,13</sup> which clearly indicates that the as-synthesized ZnO nanotubes are n-type.<sup>19</sup>

The detailed features of the piezoelectric output can be examined by the line profile traced following the AFM tip. Fig. 5c and d display two typical examples of an overlapped plots of the recorded  $z$ -height topography image (blue line) and the corresponding voltage-output profile (pink line) when the AFM tip scanned across a ZnO nanotube array from the right-hand side to the left-hand side. The positions of the outer side walls are indicated by green lines. Fig. 5c shows a case that the piezoelectric potential output was generated after the AFM tip scanned over the front wall of the nanotube along the scanning direction, which means that the voltage peak was generated when the tip just touched the inside of the tube. Fig. 5d shows another case that the piezoelectric potential output was generated after the AFM tip scanned over the backside wall of the nanotube along the scanning direction, which means that the tip scanned to the outside of the tube and was leaving the tube.

To help us understand the data presented in Fig. 5, we numerically calculated the piezoelectric potential distribution in a ZnO nanotube by mechanically deforming its shape from the top edge. For simplicity of the calculation, we ignored the doping in ZnO, which can give a reasonable result that guides our qualitative understanding.<sup>20</sup> In our calculation, a constant "point" force of  $13.9 \text{ nN}$  normal to the nanotube was maintained

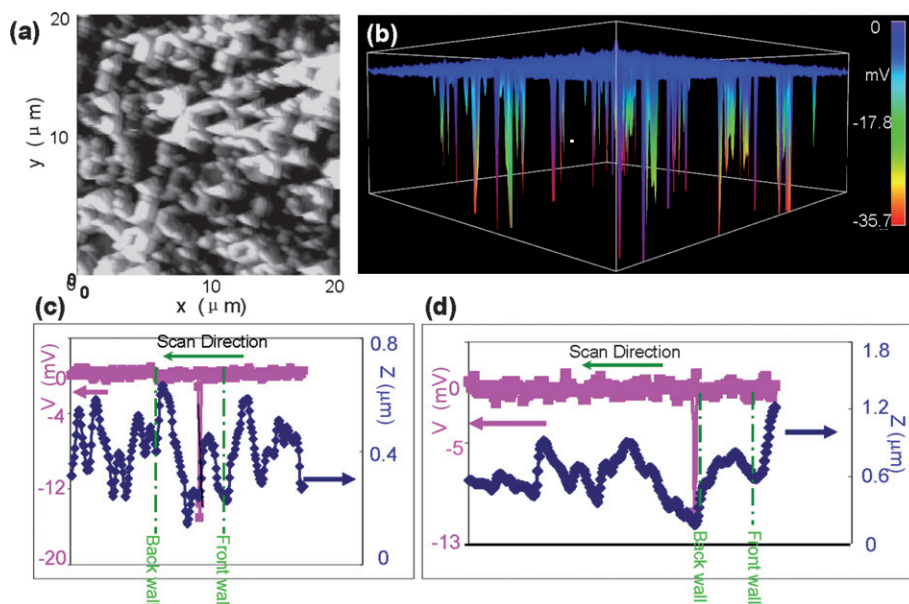


**Fig. 5** The nanogenerator based on ZnO nanotube arrays. (a) A 3D AFM topographic image taken by scanning the tip in contact mode over an area  $20 \mu\text{m} \times 20 \mu\text{m}$ . The scanning direction was from the right-hand side to the left-hand side. (b) The corresponding 3D plot of the voltage output image measured across an external load in reference to the grounded substrate. (c, d) Overlapped plots of line-scan profiles from the topography image (blue line) and the corresponding output voltage image (pink line), showing the relative position of the voltage peak in reference to the front and back walls of the nanotube.

at the top end of the tube; the inner and outer diameters of the ZnO nanotube were 800 nm and 1000 nm, respectively, and its length is  $12 \mu\text{m}$ . The ZnO nanotube constants used in the calculation are anisotropic elastic constants  $c_{11} = 209.714 \text{ GP}$ ,  $c_{12} = 121.14 \text{ GP}$ ,  $c_{13} = 105.359 \text{ GP}$ ,  $c_{22} = 209.714 \text{ GP}$ ,  $c_{23} = 105.359 \text{ GP}$ ,  $c_{33} = 211.194 \text{ GP}$ ,  $c_{44} = 43.3729 \text{ GP}$ ,  $c_{55} = 42.3729 \text{ GP}$ ,  $c_{66} = 44.2478 \text{ GP}$ , piezoelectric constants  $e_{15} = -0.480508 \text{ C m}^{-2}$ ,  $e_{24} = -0.480508 \text{ C m}^{-2}$ ,  $e_{31} = -0.567005 \text{ C m}^{-2}$ ,  $e_{32} = -0.567005 \text{ C m}^{-2}$ ,  $e_{33} = 1.32044 \text{ C m}^{-2}$ , relative dielectric constants  $\epsilon_{11} = 8.5446$ ,  $\epsilon_{22} = 8.5446$ ,  $\epsilon_{33} = 10.204$ , and the

density  $\rho = 5680 \text{ Kg m}^{-3}$ . Fig. 6a shows the finite element calculated piezoelectric potential distribution in the nanotube. The potential is output from the side view of the nanotube and the color code represents the distribution of the piezopotential, with red positive and blue negative. The result agrees to that of ZnO nanowire.<sup>19</sup> The magnitude of the positive piezopotential would be largely suppressed if we consider the n-type doping in the nanotube,<sup>21</sup> but the current result is good enough for us to qualitatively understand the trend of the measured output voltage

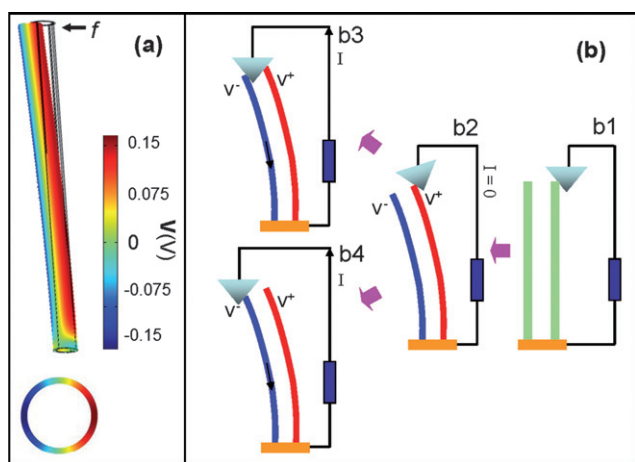


**Fig. 6** (a) Numerically calculated piezoelectric potential distribution in a ZnO nanotube without considering doping. The bottom is the piezopotential in the cross-section plane of the tube. (b) Schematic diagrams showing the possible potential output process from a nanotube as deformed by an AFM tip with the presence of a Schottky contact between the tip and the ZnO (see text for details).

Based on the calculated result presented in Fig. 6a, the piezoelectricity output process for the n-type ZnO nanotube is schematically shown in Fig. 6b. For simplicity, we use the cross-section image of the tube to represent its contact with the AFM tip. The tip height was automatically adjusted based on the tubular morphology and the local contacting force when the tip was scanned over the top of the ZnO nanotube arrays. The initial status of the tube and the tip is shown in Fig. 6b1. Once the tip pushes the tube and deforms its shape, the back and front walls of the tube has a negative and positive piezopotential (Fig. 6b2), respectively. Since the Pt coated tip and the n-type ZnO has a Schottky contact, the positive piezopotential ( $V^+$ ) wall sets the front-wall contact as reversely biased, while the negative piezopotential ( $V^-$ ) wall sets the back-wall contact as forward biased. Two possible cases can occur for current generation. The first case is that the tip immediately drops into the dip of the tube right after scanning over the front wall (Fig. 6b3). Note the apex angle of the tip is rather large, so that it is possible that the tip touches the two walls when it is located right in the tube before the tube rebounds its shape, provided the scanning speed is fast enough to catch the local piezopotential before it disappears. In such a case, the negative piezopotential  $V^-$  at the back wall results in a transient current flow through the load from the

grounded root, resulting in a negative output voltage pulse; and the position of the piezoelectric output is located between the profiles of the front and back walls of the tube in the AFM topological image. This is the case observed experimentally in Fig. 5c.

Alternatively, if the tip jumps over the tube and directly touches the back wall as in the case shown in Fig. 6b4, a similar negative output voltage pulse is observed, and the position of the piezoelectric output is located outside the profiles of the front and back walls of the tube in the AFM topological image. This is the case observed experimentally in Fig. 5d.

In our experiments, we did not observe the case where a single nanotube produces two piezoelectric output voltage pulses. This is reasonable because the cases shown in Fig. 6b3 and 6b4 cannot occur for the same tube. Only one piezoelectric discharge peak is expected to be observed for one nanotube.

## Conclusion

Hexagonal ZnO nanotube arrays were synthesized by a low-temperature solution chemical method. The morphologies of the ZnO nanotube arrays were studied under different growth conditions, such as the growth time, the growth temperature and the concentration of the nutrient solution. Piezoelectric nanogenerators using ZnO nanotube arrays were demonstrated for the first time. The characteristics of the output voltage have been studied in reference to the numerically calculated piezopotential, and the mechanism is consistent with that proposed for nanowires.<sup>2,12</sup> Our conclusion is that ZnO nanotubes can also be applied for harvesting mechanical energy.

## Acknowledgements

This research was supported by DARPA (Army/AMOCOM/REDSTONE AR, W31P4Q-08-1-0009), BESDOE (DE-FG-02-07ER46394), Air Force Office (FA9550-08-1-0046), DARPA/ARO W911NF-08-1-0249, KAUST Global Research

Partnership, and NSF. Yi Xi and Zhiyuan Gao thank the partial fellowship supported by the China Scholarship Council (CSC) (No. 20083019). Chenguo Hu and Yi Xi thanks the fund of NSFC (60976055) and Postgraduates' Science and Innovation Fund (200801CIA0080267) of Chongqing University.

## References

- 1 D. Tilman, R. Socolow, J. A. Foley, J. Hill, Eric Larson, L. Lynd, S. Pacala, J. Reilly, T. Searchinger, C. Somerville and R. Williams, *Science*, 2009, **325**, 270.
- 2 Z. L. Wang and J. Song, *Science*, 2006, **312**, 242.
- 3 X. Wang, J. Song, J. Liu and Z. L. Wang, *Science*, 2007, **316**, 102.
- 4 T. Kamiya and M. Kawasaki, *MRS Bull.*, 2008, **33**, 1061.
- 5 H. Guo, J. Zhou and Z. Lin, *Electrochem. Commun.*, 2008, **10**, 146.
- 6 Z. L. Wang, *Adv. Funct. Mater.*, 2008, **18**, 3553.
- 7 S. Xu, Y. G. Wei, M. Kirkham, J. Liu, W. J. Mai, D. Davidovic, R. L. Snyder and Zhong Lin Wang, *J. Am. Chem. Soc.*, 2008, **130**, 14958.
- 8 B. Weintraub, Y. L. Deng and Z. L. Wang, *J. Phys. Chem. C*, 2007, **111**, 10162.
- 9 Y. G. Wei, Y. Ding, C. Li, S. Xu, J. H. Ryo, R. Dupuis, A. K. Sood, D. L. Polla and Z. L. Wang, *J. Phys. Chem. C*, 2008, **112**, 18935.
- 10 Y. Xi, C. G. Hu, X. Y. Han, Y. F. Xiong, P. X. Gao and G. B. Liu, *Solid State Commun.*, 2007, **141**, 506.
- 11 J. R. Morber, X. D. Wang, J. Liu, R. L. Snyder and Z. L. Wang, *Adv. Mater.*, 2009, **21**, 2072.
- 12 J. Song, J. Zhou and Z. L. Wang, *Nano Lett.*, 2006, **6**, 1656.
- 13 S. Xu, Y. G. Wei, J. Liu, R. S. Yang and Z. L. Wang, *Nano Lett.*, 2008, **8**, 4027.
- 14 S. Xu, C. S. Lao, B. Weintraub and Z. L. Wang, *J. Mater. Res.*, 2008, **23**, 2072.
- 15 A. Wei, X. W. Sun, C. X. Xu, Z. L. Dong, Y. Yang, S. T. Tan and W. Huang, *Nanotechnology*, 2006, **17**, 1740.
- 16 L. Vayssieres, K. Keis, A. Hagfeldt and S. E. Lindquist, *Chem. Mater.*, 2001, **105**, 3350.
- 17 Q. J. Yu, W. Y. Fu, C. L. Yu, H. B. Yang, R. H. Wei, M. H. Li, S. K. Liu, Y. M. Sui, Z. L. Liu, M. X. Yuan and G. T. Zou, *J. Phys. Chem. C*, 2007, **111**, 17521.
- 18 F. Li, Y. Ding, P. X. Gao, X. Q. Xin and Z. L. Wang, *Angew. Chem.*, 2004, **116**, 5350.
- 19 S. S. Lin, J. H. Song, Y. F. Lu and Z. L. Wang, *Nanotechnology*, 2009, **20**, 365703.
- 20 Y. F. Gao and Z. L. Wang, *Nano Lett.*, 2007, **7**, 2499.
- 21 Y. F. Gao and Z. L. Wang, *Nano Lett.*, 2009, **9**, 1103.